inset into the signal strip of the CPW feed line, and the inset tuning stub has a central conducting strip of width T and length L_S, with its one end shorted to the ground plane. The gap width between the central conducting strip and the signal strip of the CPW feed line is also selected to be G, the same as the gap width of the CPW feed line. From experimental studies, it is found that the inset length (L_S) of the tuning stub is also about 0.25 guided wavelength of the center operating frequency. For the proposed design, two near-degenerate resonant modes for CP radiation can be excited, and due to the bent tuning stub protruding from the circular patch in the $\hat{x}$-direction, the excited $\hat{x}$-directed patch surface current path is expected to be lengthened, with the one in the $\hat{y}$-direction slightly affected. This phenomenon can result in left-hand CP radiation [4]. On the other hand, when the bent tuning stub protrudes from the circular patch in the $\hat{y}$-direction, right-hand CP radiation can be obtained.

The proposed CPW-fed microstrip antenna for CP radiation has been implemented. The diameter of the circular patch is 32 mm, and the width and length of the coupling slot are chosen to be 1 and 16 mm, respectively. The typical measured return loss and axial ratio are, respectively, shown in Figures 2 and 3. Good impedance matching of the CP radiation is obtained, and the impedance bandwidth (10 dB return loss) is found to be 108 MHz or about 4.3% with respect to the center frequency at 2490 MHz, which is defined to be the frequency with the minimum axial ratio in this study. The CP bandwidth, determined from the 3 dB axial ratio, is found to be 34 MHz or 1.36%. These results are comparable to those observed in [3]. Figure 4 also plots the measured radiation patterns in two orthogonal planes at 2490 MHz, and good left-hand CP radiation is observed.

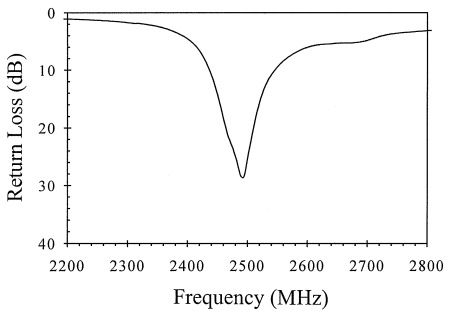

Figure 2 Measured return loss against frequency for the antenna design shown in Figure 1; $\varepsilon_r = 4.4$, $h = 1.6$ mm, $S = 6.37$ mm, $T = 1.6$ mm $= 0.28S$, $G = 0.5$ mm, $L = 16$ mm, $L_S = 18.9$ mm, $D = 32$ mm, $l = 9$ mm, $W = 1$ mm, ground-plane size = 120 mm × 120 mm

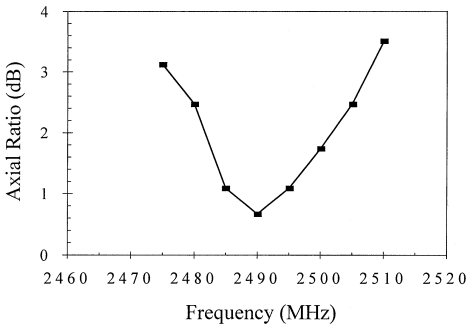

Figure 3 Measured axial ratio in the broadside direction against frequency; antenna parameters are given in Figure 2

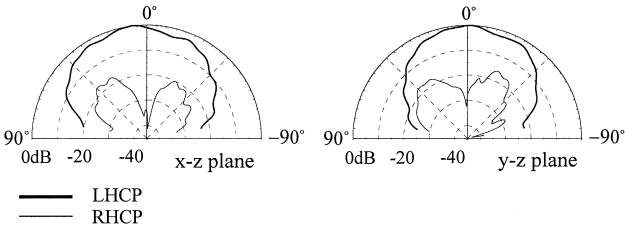

Figure 4 Measured radiation patterns in two orthogonal planes at 2490 MHz; antenna parameters are given in Figure 2

3. CONCLUSIONS

A new CPW feed design for circularly polarized microstrip antennas has been proposed. The proposed CPW feed design has a tuning stub inset into the signal strip of the CPW feed line, which reduces the required area for the layout of the feed circuitry, and makes possible a compact CPW feed circuitry for CP excitation. Experimental results also demonstrate good CP performances of the proposed antenna.

REFERENCES

1. W. Menzel and W. Grabherr, A microstrip patch antenna with coplanar feed line, IEEE Microwave Guided Wave Lett 1 (1991), 340–342.
2. L. Giauffret, J.-M. Laheurte, and A. Papiernik, Study of various shapes of the coupling slot in the CPW-fed microstrip antennas, IEEE Trans Antennas Propagat 45 (1997), 642–646.
3. C.Y. Huang and K.L. Wong, Coplanar waveguide-fed circularly polarized microstrip antenna, IEEE Trans Antennas Propagat 48 (2000), 328–329.
4. K.L. Wong and M.H. Chen, Small slot-coupled circularly-polarized microstrip antenna with modified cross-slot and bent tuning-stub, Electron Lett 34 (1998), 1542–1543.

ANALYSIS OF RESONANCE PROCESSES IN MICROSTRIP RING RESONATORS BY THE FDTD METHOD

Elena Semouchkina,[1] Wenwu Cao,[1,2] Raj Mittra,[3] and Wenhua Yu[3]

[1] Materials Research Laboratory
The Pennsylvania State University
University Park, Pennsylvania 16802
[2] Department of Mathematics
The Pennsylvania State University
University Park, Pennsylvania 16802
[3] Department of Electrical Engineering
The Pennsylvania State University
University Park, Pennsylvania 16802

Received 11 September 2000

ABSTRACT: *In this paper, the finite-difference time-domain method is used to analyze resonance processes in microstrip ring resonators, which are either edge or side coupled to the feedlines, in both the time and frequency domains. Standing waves established in resonant structures are visualized by simulating the spatial distribution of electromagnetic fields*

Contract grant sponsor: Center for Dielectric Studies of The Pennsylvania State University

at resonant frequencies. The wave processes, which determine the resonance formation in edge- and side-coupled resonators, are found to be significantly different in these two structures. © 2001 John Wiley & Sons, Inc. Microwave Opt Technol Lett 28: 312–321, 2001.

Key words: *microwave resonator; microstrip ring; finite-difference time-domain method; electromagnetic waves; resonance*

1. INTRODUCTION

Microstrip ring resonators are widely used in many microwave devices, particularly in filters, mixers, oscillators, and couplers [1]. The interest of researchers and commercial communication industry engineers to these structures has recently increased due to the application of ferroelectric thin-film substrates and high-temperature superconducting microstrip lines in ring resonator fabrication [2, 3]. The microwave components based on such structures have smaller size, lighter weight, a higher Q-factor because of the superconductivity of microstrips, and are tunable due to the sensitivity of the substrate to changes in dc electric fields. An important aspect of ring resonator investigation is to modify its design in order to perform selective mode damping without an increase in topological area [4, 5]. Another goal is to achieve frequency tunability through design modification, as in split-ring resonators [6]. In order to successfully integrate new microstrip ring components into communication systems, it is very important to have a clear understanding of the resonance processes in ring resonators, and to model their responses adequately. However, the analysis of ring resonators has been carried out primarily by using transmission-line theories [7, 8], and within the context of the quasi-TEM approximation [9, 10]. This approach is rather limited; it cannot be used either for arbitrary microstrip geometries or for a large dielectric constant of the substrate, and is not appropriate for high frequencies. Previously, we have successfully implemented the full-wave modeling of microstrip ring resonators using the finite-difference time-domain (FDTD) method, have simulated the S-parameter spectra of ring resonators, and have demonstrated that the simulation results agree well with experimental measurements [11].

In this paper, we use the FDTD simulations of electromagnetic fields in the time domain to study the wave-propagation process and the frequency-domain analysis of the fields to visualize standing waves in edge- and side-coupled ring resonators. The simulation of standing-wave patterns is very important for ring resonator design modification.

2. SIMULATION PROCEDURE

Both the edge-coupled [Fig. 1(a)] and side-coupled [Fig 1(b)] ring resonators with rutile substrates (relative dielectric constant equal to 98) were simulated. The thickness of the rutile layer is 1.5 mm. The dimensions of the resonators are the same as those in the experimental samples that were measured previously [11]. The conductive ring and the feedlines are 0.25 mm wide, with an outside diameter of 10 mm. The coupling gaps in the edge-coupled ring resonator and the minimum distance to the feedline in the side-coupled ring resonator are both equal to 0.125 mm. The conformal FDTD technique [12], which allows one to model infinitely thin perfectly conducting curved surfaces without resorting to a staircasing approximation, was used in the simulations. Perfectly matched layer (PML) boundary conditions [13] were applied at all surfaces of the computational domain, except

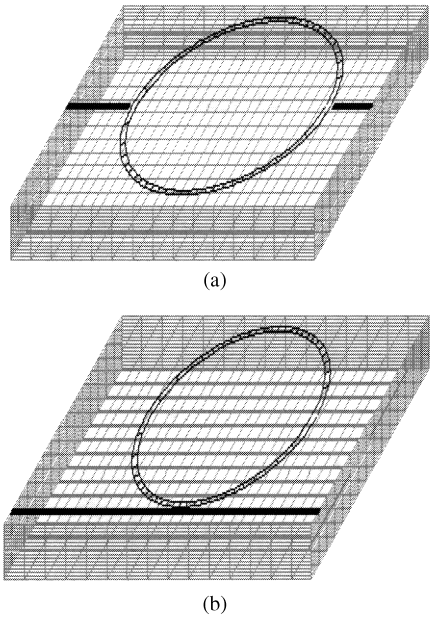

Figure 1 Geometries of ring resonators. (a) Edge-coupled ring resonator. (b) Side-coupled ring resonator

that a perfectly conducting ground plane was put at the bottom substrate surface. A Gaussian-shaped electric-field pulse with a bandwidth of 10 GHz modulated by a sinusoidal wave of 5 GHz was applied between the microstrip feedline and the ground plane at a distance of 0.625 mm from the left PML boundary to excite ring resonators. The fast Four transformation (FFT) procedure was used to simulate electromagnetic fields in frequency domain, and the spatial field distributions of these fields were plotted at several frequencies. The resonance frequencies of the structures were determined from the simulations of the S-parameter spectra [11].

3. RESULTS

Figures 2 and 3 exhibit the spatial distributions of the electric-field component normal to the substrate surface, and its contour plots at different time steps for the ring resonator which is edge coupled to the feedlines. The plane where the field distribution and its contour plots are determined is located 0.3 mm below the metal ring inside the dielectric. The plots show that the waves propagate in a microstrip ring resonator not only beneath the microstrip ring, but also outside it. Furthermore, the field levels of these traveling waves in the external region are comparable to those that are excited below the ring. The waves propagating inside the dielectric are first launched by the original excitation source, and later by the coupling gap which begins to act as a radiation source. It is also seen from the plot that the waves are propagating faster beneath the metal ring strips than outside the strips, which leads to a change of the shape of the wavefront with time. We also note from Figures 2 and 3 that the wave propagation process in the edge-coupled ring resonator, which leads to the resonance formation, consists of forward (Fig. 2) and backward (Fig. 3) repeatable movement of the wave packet between the two coupling gaps inside the ring.

Figures 4 and 5 depict, respectively, the corresponding distribution and contour plots for the edge-coupled ring

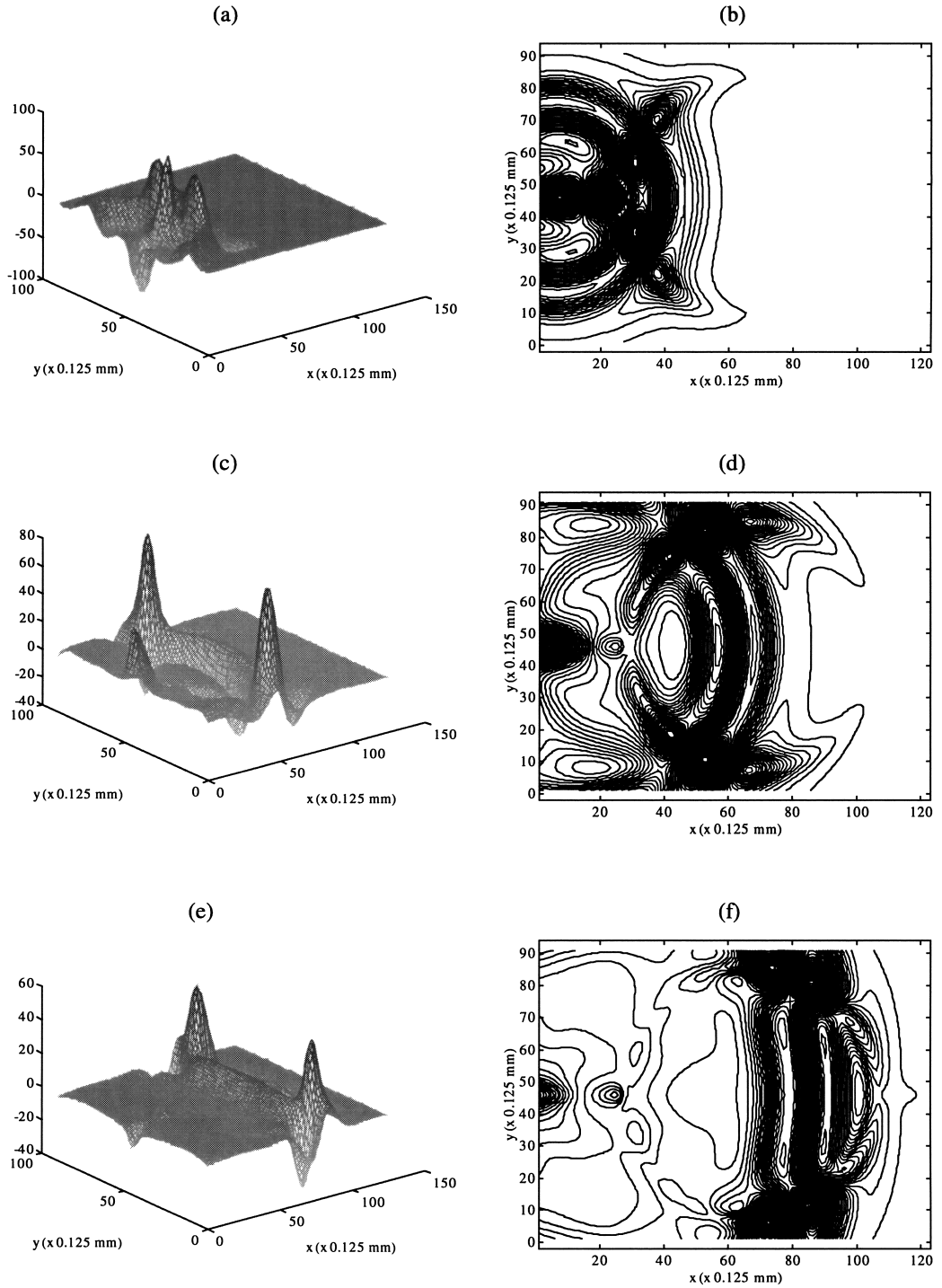

Figure 2 Distribution of the electric-field component normal to the substrate surface in the plane located 0.3 mm below the metal ring (a), (c), (e) and its contour plots (b), (d), (f) in the edge-coupled ring resonator at different time step numbers N. (a), (b) $N = 1000$. (c), (d) $N = 1500$. (e), (f) $N = 2000$. Time step is equal to 0.25 ps

resonator at the first four resonance frequencies. Standing waves established in the ring resonator can be clearly observed in these pictures. The locations of the maxima and nulls of the field can be easily defined.

The results of similar simulations performed for the case of a ring resonator, side coupled to the feedline, are presented in Figures 6–9. Figures 6 and 7 present the time-domain simulations, which clearly show the wave propagating outside the microstrips, and also indicate that the wave velocities are different in the regions underneath and outside the metal ring. However, the plots also show that, in the side-coupled ring resonator, the waves do not oscillate back

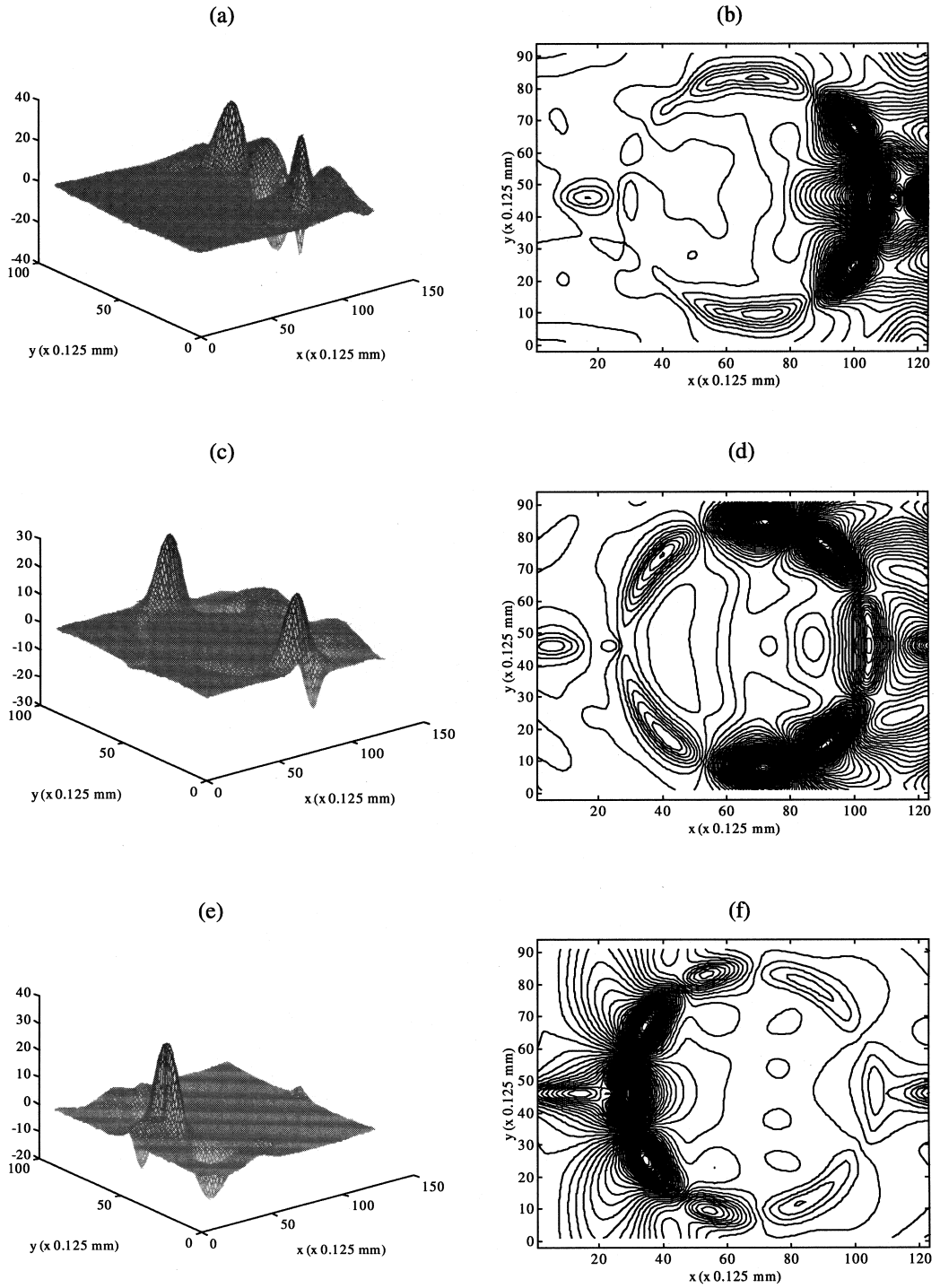

Figure 3 Distribution of the electric-field component normal to the substrate surface in the plane located 0.3 mm below the metal ring (a), (c), (e) and its contour plots (b), (d), (f) in the edge-coupled ring resonator at different time step numbers N. (a), (b) $N = 3000$. (c), (d) $N = 3500$. (e), (f) $N = 4500$. Time step is equal to 0.25 ps

and forth inside the ring, and the wave packet moves circularly along the ring instead. This circulatory movement of the wave helps form the standing wave at resonance.

Figures 8 and 9 present the field distribution and contour plots in the side-coupled ring resonator at the first four resonance frequencies. One can see that the locations of maxima and nulls of the field at resonant frequencies for the side-coupled ring resonator are shifted with respect to those of the edge-coupled ring resonator. The corresponding resonant frequencies for the edge- and side-coupled ring resonators also appear to be shifted with respect to each other for the same size rings. This resonant frequency shift increases with frequency, from 0.01 GHz for the first resonance peak to 0.18 GHz for the fourth resonance peak. The obtained results indicate that the excitation type has an influence on the process of wave propagation and standing-wave

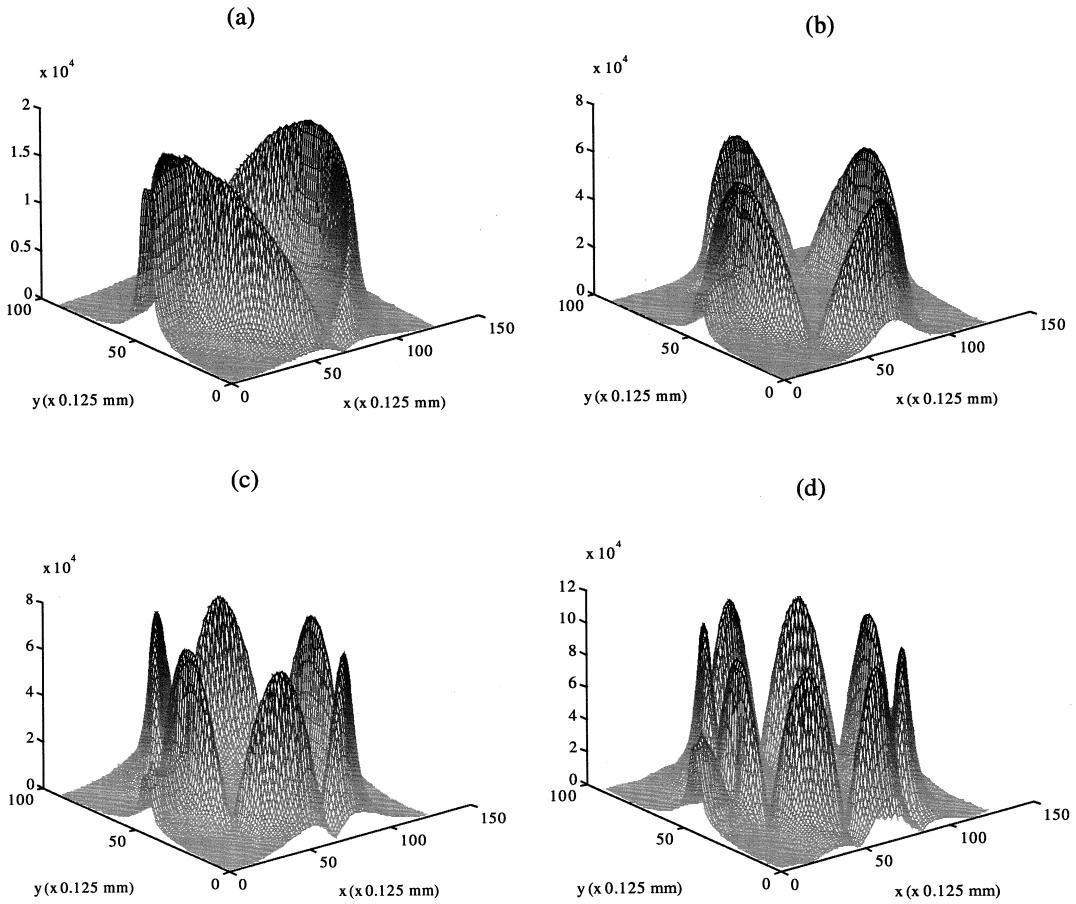

Figure 4 Distribution of the electric-field component normal to the substrate surface in the plane located 0.3 mm below the metal ring in the edge-coupled ring resonator at different frequencies f. (a) $f = 1.24$ GHz. (b) $f = 2.34$ GHz. (c) $f = 3.44$ GHz. (d) $f = 4.44$ GHz

formation in the ring resonators. While the wavelength of the standing waves is determined only by the ring dimensions, the corresponding resonant frequencies, as well as the locations of maxima and nulls of the field, are affected by the excitation type, i.e., by the path of the propagating wave.

4. CONCLUSIONS

We have simulated the wave propagation and standing-wave formation in edge- and side-coupled microstrip ring resonators with rutile substrates using the FDTD method in the time and frequency domains. It was demonstrated that the fields do propagate outside the microstrip ring in the rutile substrate, a phenomenon which cannot be predicted if the TEM approximation is used to model these fields. Plotting the frequency domain data at the resonant frequencies enabled us to visualize standing-wave patterns established in the structures. It was shown that the resonant frequencies and the locations of field maxima and nulls depend on the excitation and the path of the propagating wave. The knowledge of the locations of field maxima and nulls at resonance frequencies can be used to suppress the undesirable resonances through a modification of resonator designs, such as introducing slits at proper locations, using stepped-impedance microstrip sections, and adding coupled lines or short-circuit sections to the ground.

REFERENCES

1. K. Chang, Microwave ring circuits and antennas, Wiley, New York, 1996.
2. K.B. Bhasin, C.M. Chorey, J.D. Warner, R.R. Romanofsky, V.O. Heinen, K.S. Kong, H.Y. Lee, and T. Itoh, Performance and modeling of superconducting ring resonators at millimeter-wave frequencies, IEEE MTT-S Int Microwave Symp Dig, Part 1, Dallas, TX, 1990, vol. 1, pp. 269–272.
3. F.A. Miranda, F.W. Van Keuls, R.R. Romanofsky, and G. Subramanyam, Tunable microwave components for Ku- and k-band satellite communications, Proc 10th Int Symp Integrated Ferroelectron, Part 2, Monterey, CA, 1998, vol. 22, pp. 269–278.
4. J.-Y. Park and J.-C. Lee, New enhanced coupling structure of microstrip ring resonator with two coupled lines and a slit, IEEE MTT-S Int Microwave Symp Dig, Part 2, Baltimore, MD, 1998, vol. 2, pp. 805–808.
5. J. Marti and A. Griol, Harmonic suppressed microstrip multistage coupled ring bandpass filters, Electron Lett 34 (1998), 2140–2142.
6. D.K. Paul, P. Gardner, and K.P. Tan, Suppression of even modes in microstrip ring resonators, Electron Lett 21 (1994), 1772–1774.

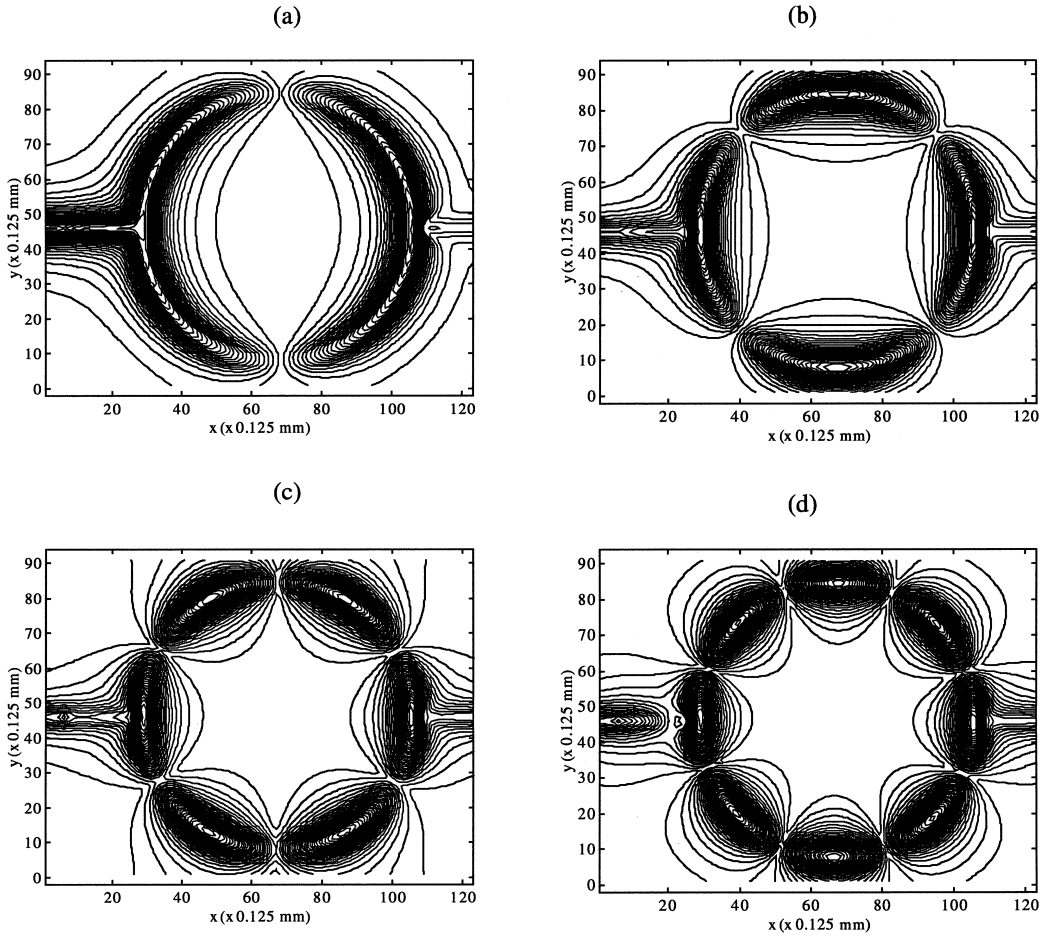

Figure 5 Contour plots of the electric-field component normal to the substrate surface in the plane located 0.3 mm below the metal ring in the edge-coupled ring resonator at different frequencies f. (a) $f = 1.24$ GHz. (b) $f = 2.34$ GHz. (c) $f = 3.44$ GHz. (d) $f = 4.44$ GHz

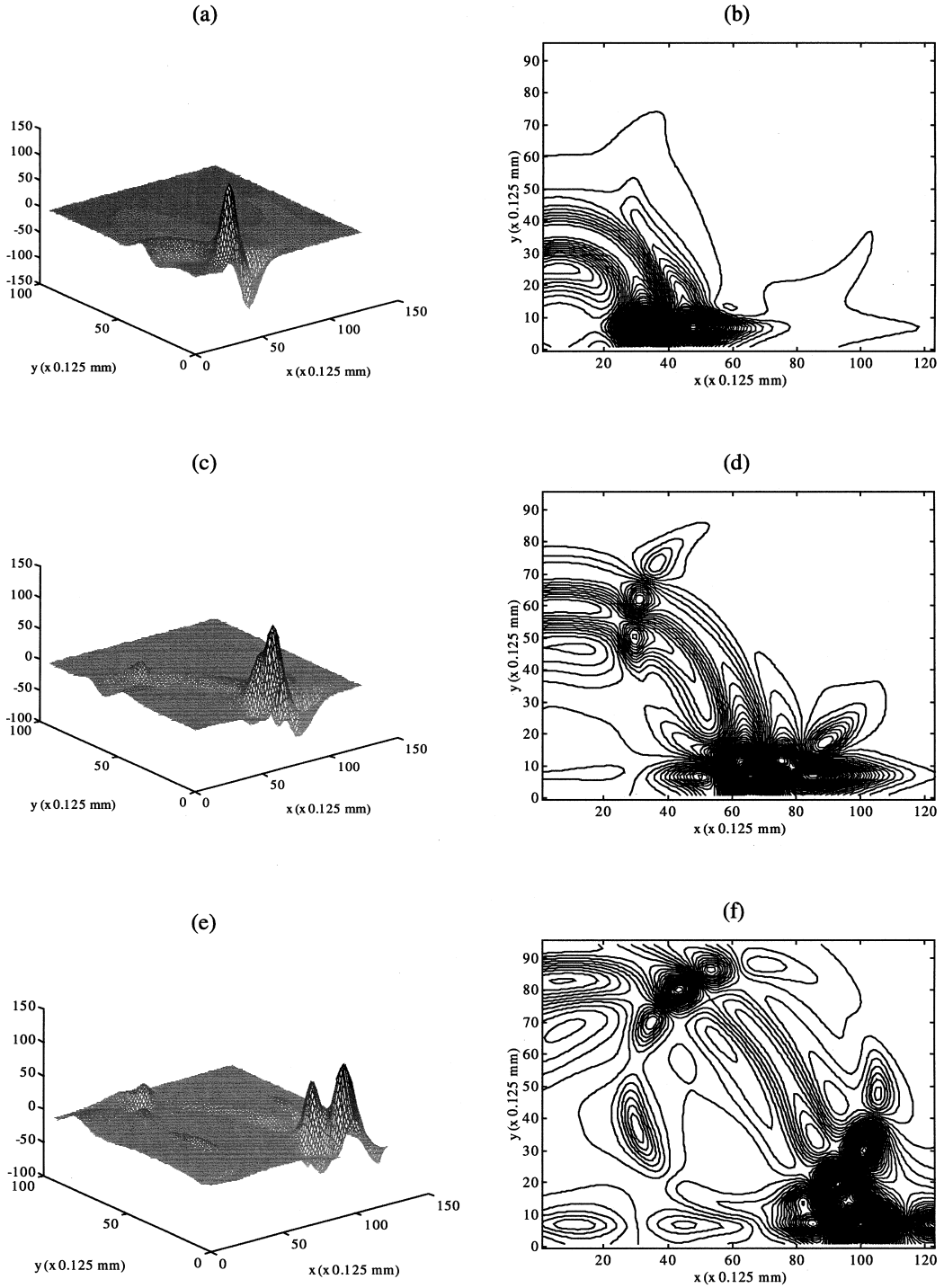

Figure 6 Distribution of the electric-field component normal to the substrate surface in the place located 0.3 mm below the metal ring (a), (c), (e) and its contour plots (b), (d), (f) in the side-coupled ring resonator at different time step numbers N. (a), (b) $N = 1000$. (c), (d) $N = 1500$. (e), (f) $N = 2000$. Time step is equal to 0.25 ps

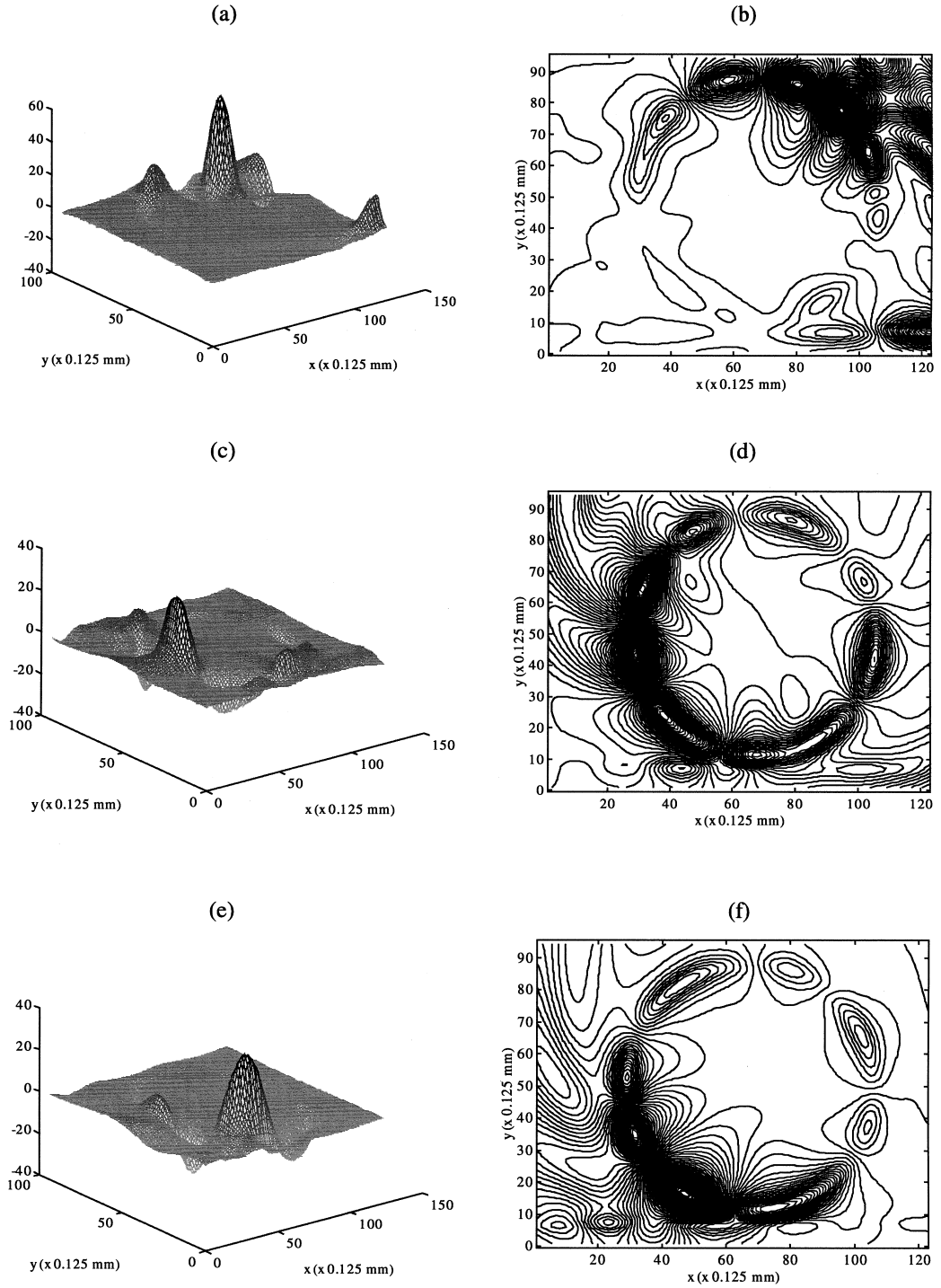

Figure 7 Distribution of the electric-field component normal to the substrate surface in the plane located 0.3 mm below the metal ring (a), (c), (e) and its contour plots (b), (d), (f) in the side-coupled ring resonator at different time step numbers N. (a), (b) $N = 3000$. (c), (d) $N = 4500$. (e), (f) $N = 5000$. Time step is equal to 0.25 ps

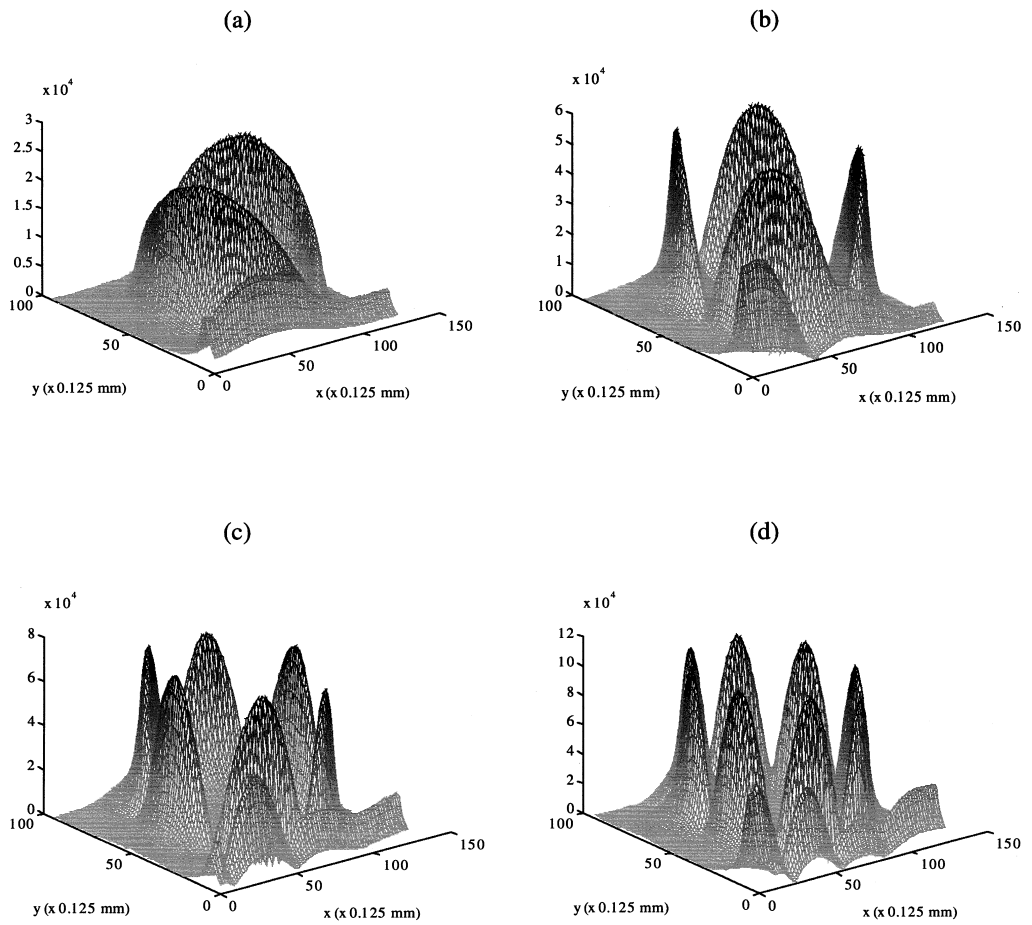

Figure 8 Distribution of the electric-field component normal to the substrate surface in the plane located 0.3 mm below the metal ring in the side-coupled ring resonator at different frequencies f. (a) $f = 1.23$ GHz. (b) $f = 2.42$ GHz. (c) $f = 3.56$ GHz. (d) $f = 4.58$ GHz

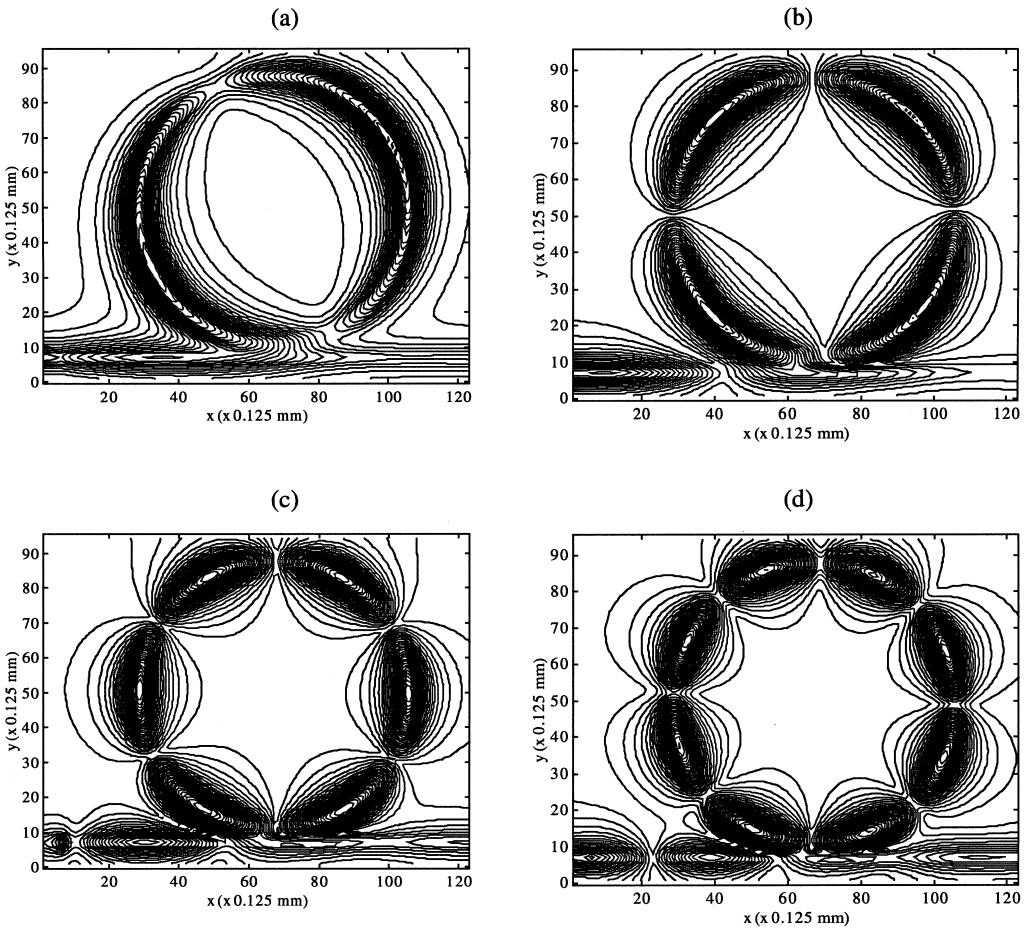

Figure 9 Contour plots of the electric-field component normal to the substrate surface in the plane located 0.3 mm below the metal ring in the side-coupled ring resonator at different frequencies f. (a) $f = 1.23$ GHz. (b) $f = 2.42$ GHz. (c) $f = 3.56$ GHz. (d) $f = 4.58$ GHz

7. C.-C. Yu and K. Chang, Transmission-line analysis of a capacitively coupled microstrip-ring resonator, IEEE Trans Microwave Theory Tech 45 (1997), 2018–2024.
8. L. Zhu and K. Wu, Line-to-strip coupling circuit model and its parametric effects for optimized design of microstrip ring circuits and antennas, IEEE MTT-S Int Symp Dig, Part 1, Denver, CO, 1997, vol. 1, pp. 289–292.
9. E.O. Hammerstad, Equations for microstrip circuit design, Proc European Microwave Conf, Hamburg, Germany, 1975, pp. 268–272.
10. I.J. Bahl and D.K. Trivedi, A designer's guide to microstrip line, Microwaves (1977), 174–181.
11. E. Semouchkina, W. Cao, and R. Mittra, Modeling of microwave ring resonators using the finite-difference time-domain method (FDTD), Microwave Opt Technol Lett 24 (2000), 392–396.
12. W. Yu and R. Mittra, Accurate modeling of planar microwave circuit using conformal FDTD algorithm, Electron Lett 36 (2000), 618–619.
13. S.D. Gedney, An anisotropic perfectly matched layer-absorbing medium for the truncation of FDTD lattices, IEEE Trans Microwave Theory Tech (1996), 1630–1639.

AN EXPERIMENTAL STUDY OF A λ/4 WAVE ABSORBER USING A FREQUENCY-SELECTIVE SURFACE

Akihiko Ito,[1] Hidetoshi Ebara,[2] Hidemi Nakajima,[1] Kouji Wada,[2] and Osamu Hashimoto[2]
[1] Technical Research Institute
Toppan Printing Company, Ltd.
Saitama 345-8508, Japan
[2] College of Science and Engineering
Aoyama Gakuin University
Tokyo 157-8572, Japan

Received 12 September 2000; revised 18 October 2000

ABSTRACT: *The aim of this paper is to study a basic characteristic of a frequency-selective surface (FSS) and its application to a λ/4 wave absorber. In this study, the shielding characteristics with frequency selection by an FSS, and the absorption and shielding characteristics of the proposed λ/4 wave absorber on the basis of an FSS are examined experimentally. Consequently, good performances of the FSS and the λ/4 wave absorber using an FSS were obtained, as expected.* © 2001 John Wiley & Sons, Inc. Microwave Opt Technol Lett 28: 321–323, 2001.

Key words: *λ/4 wave absorber; frequency-selective surface; indume–tin–oxide film; frequency selectivity*